2022 19th International Conference on Electrical Engineering, Computing Science and Automatic Control (CCE). Mexico City, Mexico. November 9-11, 2022

Backstepping Control for Tracking of Solenoid Valve Actuated Pneumatic Continuum Soft Robots

Jorge E. Ayala-Carrillo
Robotics and Advanced Manufacturing Department
CINVESTAV-IPN
Ramos Arizpe, Mexico
jorge.ayala@cinvestav.mx

Christian A. Trejo-Ramos
Robotics and Advanced Manufacturing Department
CINVESTAV-IPN
Ramos Arizpe, Mexico
christian.trejo@cinvestav.edu.mx

Ernesto Olguín-Díaz
Robotics and Advanced Manufacturing Department
CINVESTAV-IPN
Ramos Arizpe, Mexico
ernesto.olguin@cinvestav.edu.mx

Vicente Parra-Vega
Robotics and Advanced Manufacturing Department
CINVESTAV-IPN
Ramos Arizpe, Mexico
vparra@cinvestav.mx

***Abstract*—Among the different soft robot types developed, pneumatic continuum soft robots are nowadays the most widely researched type due to their highly compliant behaviour, but their modeling and control remain challenging tasks given its distribute parameters nature and the nonlinearities of its elastomer material. These nonlinearities are aggravated by considering pneumatic actuation dynamics, leading to a highly complex system. While pneumatic actuation dynamics is usually not taken in account for the design of feedback controllers, experiments have shown that they are far from negligible. In this paper, we study a highly coupled nonlinear model that relates the Lagrangian dynamics approach of a continuum soft robot and the pressure dynamics of its embedded pneumatic chambers. Then, a model-based feedback control strategy based on backstepping is proposed for the tracking of a pneumatic continuum soft robot configuration, achieving exponential stability. Finally, simulations are presented and concluding remarks are discussed.**

***Index Terms*—Backstepping control, Soft robot, Pneumatic control, Solenoid valve.**

I. Introduction

Closed-loop dynamics of a pneumatic continuum soft robot (pCSR) differs substantially from its counterpart, the rigid robot, since nonlinear material properties, infinite degrees of freedom, and model uncertainties are involved [1]. Consequently, pneumatic control techniques for rigid robots cannot be directly applied to pCSRs [2]. Therefore, to address the control design of such a system, a model incorporating the complexity of both the robot continuum deformation and pneumatic actuation dynamics is needed. Nevertheless, some works have addressed pCSR control design by assuming 1) a simplified robot deformation dynamics [3] or 2) neglecting pneumatic dynamics [4]. Thus, while there is a healthy amount of literature on pneumatic control [5] and on soft robots [2], [6], the pneumatic control for pCSR with complete dynamics is still an open problem in the literature of soft robotics. Model-based control has been currently explored for pCSRs because of its advantages in efficiency and accuracy, despite its downside regarding practical viability and complexity to implement [7]. In our previous work [8], we proposed a pneumatic controller that guarantees robust configuration tracking for a cascade system considering pCSR complete dynamics, with finite-time convergence of pressure tracking errors; the results were adequate, but we noticed that the coupled nonlinear dynamics also suggest a control design by the backstepping techinque. Backstepping is a well-known control strategy particularly useful for dynamical systems with a nonlinear triangular structure [9], [10] and underactuation [11]. This strategy has already been addressed to deformable body systems equipped with pneumatic actuation, [12], [13], [14]. Notably, [12] proposes a backstepping control for a one degree of freedom soft bending arm actuated by solenoid valves. For a pneumatic soft robot driven by solenoid valves, [13] propose an energy-based control scheme compared to a backstepping controller, but soft robot dynamics is approximated through 3 rigid links. The approach of [14] shows a backstepping design for an underactuated piston-driven piecewise constant curvature soft robot, with the disadvantage of limiting input pressure by the piston volume. Actuation for a pCSR is usually adressed with solenoid valves, see [15] a comparison between proportional and PWM solenoid valves for soft actuators; therefore, it sounds reasonable to address the pneumatic control of pCSR assuming solenoid valves and the complete continuum soft robot dynamics.

1) Contribution: In this paper, we design a backstepping control for a solenoid valve actuated pCSR, therefore, the dynamics of this coupled system is also addressed. The pCSR dynamics, under proper assumptions, is parameterized through three deformation parameters; then if three embedded pneumatic chambers (evenly distributed) are considered, a fully actuated system with a strict feedback structure is achieved. Hence, the backstepping algorithm can be applied to design the control to stabilize the pCSR dynamics.

2) Organization: System modeling is detailed in Section II. First, pCSR dynamic model is derived, next, the pneumatic system dynamics is obtained and the coupled system considering both models is presented and used to state the control problem. In Section III, the dynamic model is expressed in error coordinates the backstepping algorithm is applied to derive the control law in accordance to the stability analysis. Simulations exemplify a case study in Section IV, and discussions are addressed in Section V. Conclusions are given in Section VI.

We greatly acknowledge Conacyt-Mexico for Graduate Scholarships #1076387 and #737439 granted to the first and second authors.

978-1-6654-5508-4/22/$31.00 ©2022 IEEE

II. MODELING

A. Assumptions

On one hand, the pCSR can be considered as deformable body that produces motion through controlled deformation by internal pneumatic chambers. Such characteristic provides in principle infinite degrees of freedom (DoF's) to the pCSR; moreover, we introduce the following assumptions:

- A1 Relative distance among particles is not constant.
- A2 Radial and circumferential deformation are constrained.
- A3 There is a backbone line representing body deformation.

With this assumptions, a Lagrangian-like finite dimension representation of the pCSR can be obtained as follows, [16]

$$H(\boldsymbol{q})\ddot{\boldsymbol{q}} + C(\boldsymbol{q},\dot{\boldsymbol{q}})\dot{\boldsymbol{q}} + \boldsymbol{\tau}_{vs} + \boldsymbol{g}(\boldsymbol{q}) = \boldsymbol{\tau} \tag{1}$$

where $\boldsymbol{q}, \dot{\boldsymbol{q}}$ are the state of position and velocity deformation coordinates, $H(\boldsymbol{q})$ the inertial matrix, $C(\boldsymbol{q},\dot{\boldsymbol{q}})\dot{\boldsymbol{q}}$ the Coriolis vector, $\boldsymbol{\tau}_{vs}$ models viscoelastic forces, and $\boldsymbol{g}(\boldsymbol{q})$ gravitation loads; and $\boldsymbol{\tau}$ the control input. On the other hand, this soft robot is driven by embedded pneumatic chambers, whose dynamics is developed under the additional assumptions:

- A4 There are no air leaks.
- A5 The gas inside the chamber is perfect and behaves according to the ideal gas law.
- A6 The pneumatic actuation is isentropic process.
- A7 The pressure and temperature in the chamber is homogeneous.

Now, we develop the expresions of both soft robot (1) and its actuation pneumatic dynamics.

B. Soft Robot Dynamics

1) Inertial Matrix: Soft robot dynamics is derived using the Lagrangian formalism under A1-A3 to obtain the classical Lagrangian structure (1), except for viscoelastic forces $\boldsymbol{\tau}_{vs}$ which is a subject beyond our proposal. Now, let $\boldsymbol{q} = (l,\ \phi,\ \kappa)^T \in \mathbb{R}^3$ represent the set of generalized deformation coordinates of length, azimuth and curvature of the backbone line, respectively, see Fig. 1). Notice that both the positive definite symmetric inertia matrix $H(\boldsymbol{q}) = \int_b J_p^T(\cdot)J_p(\cdot)dm \in \mathbb{R}^{n\times n}$ and gravity potential energy $U_g(\boldsymbol{q}) = -\int_b(\boldsymbol{r}_p(\boldsymbol{q})\cdot\boldsymbol{g}_0)dm$ depend on a particle position vector $\boldsymbol{r}_p(\boldsymbol{q}) \in \mathbb{R}^3$ and its Jacobian $J_p(\boldsymbol{q}) = \partial\boldsymbol{r}_p/\partial\boldsymbol{q}$, and both require body mass integration. Particle position vector of a pCSR is [16]

$$\boldsymbol{r}_p(\boldsymbol{q},\boldsymbol{b}) = \frac{1}{\kappa}\begin{pmatrix} C_\phi + C_{\bar\theta}C_\phi\left(\kappa r C_{\phi-\psi} - 1\right) + \kappa r S_\phi S_{\phi-\psi} \\ S_\phi + C_{\bar\theta}S_\phi\left(\kappa r C_{\phi-\psi} - 1\right) - \kappa r C_\phi S_{\phi-\psi} \\ \left(1 - \kappa r C_{\phi-\psi}\right) S_{\bar\theta} \end{pmatrix},$$

where $C_x = \cos x$, $S_y = \sin y$, $\bar\theta = \kappa l s$, and $\boldsymbol{c} = (r,\ \psi,\ s)^T \in \mathbb{R}^3$ are the set of toroidal coordinates composed of an $s-$variable $\in [0,1]$ (a measure along the backbone line), and a pair of polar coordinates $(r,\psi) \in [0, r_o] \times [-\pi,\pi]$, with r_o as the outer cylindrical radius of the soft body. These coordinates are used to compute body mass integration (dm) as a volume integral (dV) incorporating a variable density function, see [16].

2) Coriolis Matrix: The Coriolis matrix $C(\boldsymbol{q},\dot{\boldsymbol{q}}) \in \mathbb{R}^{n\times n}$ in (1), is computed with Christoffel symbols after the inertia matrix elements.

3) Gravity Vector: Gravity vector $\boldsymbol{g}(\boldsymbol{q}) = \partial U_g/\partial\boldsymbol{q} \in \mathbb{R}^n$, for $\boldsymbol{g}_0 = (0\,0\ -9.81\text{m/s}^2)^T$ the gravity acceleration vector.

4) Control Input: The exogenous input $\boldsymbol{\tau} \in \mathbb{R}^n$ stands for the generalized force control vector produced by p pneumatic actuators. Let a set of p *relative pressure* inputs $\boldsymbol{P}_r = (p_{1_r},\ p_{2_r}\cdots, p_{p_r})^T \in \mathbb{R}^p$ be associated to pneumatic embedded chambers that produce $\boldsymbol{\tau} = B_q(\boldsymbol{q})\boldsymbol{P}_r$, where $B_q(\boldsymbol{q}) = [\ \cdots\ \partial V_i(\boldsymbol{q})/\ \partial\boldsymbol{q}\ \cdots\ ] \in \mathbb{R}^{n\times p}$ is the well-posed (full rank) input matrix with $V_i(\boldsymbol{q})$ as the ith chamber's volume, see next subsection.

5) Viscoelastic Forces: Special attention is devoted to the viscoelastic forces term $\boldsymbol{\tau}_{vs} \in \mathbb{R}^n$ that arise all along the deformable bodies and these represent the internal forces due to deformations of internal particle motions. Precise models are beyond the scope of this work, but it suffices now to consider, without loss of generality, the Kelvin-Voigt model [17]: $\boldsymbol{\tau}_{vs} = D\dot{\boldsymbol{q}} + K_e\bar{\boldsymbol{q}} \in \mathbb{R}^n$ for order-n positive semi-definite matrices $(D, K_e) \geq 0$.

C. Pneumatic System Dynamics

By virtue of the ideal gas law, and after A4-A7, the pressure dynamics for a rigid pneumatic chamber (such as a pneumatic piston) is, [18],

$$\dot P + \frac{\dot V}{V}P = \frac{RT}{V}\dot m \tag{2}$$

where P is the *absolute pressure* in the chamber, V is the chamber's volume, R stands for the ideal gas constant, T as the temperature, and $\dot m$ is the mass flow rate –with m the air mass inside the chamber–. Assuming reasonably that $V > 0$ as in a conventional physical context, the volume of the rigid pneumatic chamber varies due to linear displacement. However, the volume changes after any displacement on a deformable pneumatic chamber. Consequently, the internal volume of each deformable pneumatic chamber embedded into the pCSR can be modeled as a function of the generalized coordinates. For cylindrical chambers with cross section area a_{ch_i} and (ψ_i, r_{m_i}) the centroid's constant polar coordinates over the toroidal cross section area of the pCSR, the chamber volume $V_i(\boldsymbol{q})$ and its time derivative $\dot V_i(\boldsymbol{q},\dot{\boldsymbol{q}})$ are given as follows, [16]:

$$V_i(\boldsymbol{q}) = a_{ch_i} l\left(1 - \kappa r_{m_i} C_{\psi_i-\phi}\right) > 0, \tag{3}$$

$$\begin{aligned}\dot V_i(\boldsymbol{q},\dot{\boldsymbol{q}}) = a_{ch_i}\big(&\dot l\left(1 - \kappa r_{m_i} C_{\psi_i-\phi}\right) - l\kappa r_{m_i}\dot\phi S_{\psi_i-\phi} \\ &- l r_{m_i}\dot\kappa C_{\psi_i-\phi}\big)\end{aligned} \tag{4}$$

where $\dot V_i(\boldsymbol{q},\dot{\boldsymbol{q}})$ is sign undefined.

Notice that since the volume is now function of the generalized coordinates, then it varies along coordinates l and κ, which implies that additional non-negligible dynamical couplings arise at dynamical level. It is easy to extend (2) for p chambers as

$$\dot{\boldsymbol{P}} + V^{-1}(\boldsymbol{q})\dot V(\boldsymbol{q},\dot{\boldsymbol{q}})\boldsymbol{P} = \rho_0\, R\, T\, V^{-1}(\boldsymbol{q})\boldsymbol{Q}, \tag{5}$$

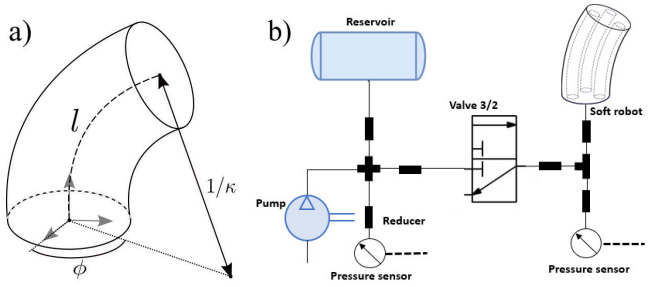

Fig. 1. a) pCSR deformation coordinates. b) Electro-pneumatic circuit for a pneumatic chamber of the pCSR.

with entry-wise vectors $(\boldsymbol{P}, \dot{\boldsymbol{m}}, \boldsymbol{Q}) \in \mathbb{R}^p$ and entry-wise diagonal matrices $[V(\boldsymbol{q})(\boldsymbol{q}), \dot{V}(\boldsymbol{q}, \dot{\boldsymbol{q}})(\boldsymbol{q})] \in \mathbb{R}^{p\times p}$; where the mass flow rate vector has been replaced with $\dot{\boldsymbol{m}} = \rho_0 \boldsymbol{Q}$, for ρ_0 (the air density at reference conditions) and the volumetric flow vector $\boldsymbol{Q}$.

The electro-pneumatic system [19], shown in Fig. 1, includes a pressure reservoir (set at $P_R \in \mathbb{R}_+$) to comply to the ISO 6358 standard, [20], by defining the volumetric flow supplied by solenoid valves as

$$\mathbf{Q} = C\Psi(\cdot)\boldsymbol{u}, \tag{6}$$

with $\boldsymbol{u} \in \mathbb{R}^p$ representing the control pressure vector as a factor of the upstream pressure, C the sonic conductance, and $\Psi \in \mathbb{R}^{p\times p}$ a diagonal positive definite flow matrix whose diagonal elements are of the form

$$\bar{\psi}_i = \begin{cases} 1 & \text{if} \quad \varphi_i < b, \quad \text{(choked)} \\ \sqrt{1 - \left(\dfrac{\varphi_i - b}{1-b}\right)^2} & \text{if} \quad \varphi_i \geq b, \quad \text{(subsonic)} \end{cases} \tag{7}$$

where $\varphi_i = p_{d_i}/p_{u_i}$ is the $i-th$ piece-wise ratio between downstream absolute pressure coordinates $\boldsymbol{P}_d = (p_{d1},\ p_{d2}\cdots, p_{dp})^T \in \mathbb{R}^p$ and upstream absolute pressure coordinates $\boldsymbol{P}_u = (p_{u1},\ p_{u2}\cdots, p_{up})^T \in \mathbb{R}^p$, and b is the critical pressure ratio at which the air reaches sonic speed at the nozzles. Notice that b and C are values dependant of each solenoid valve.

The values of the upstream coordinates p_{u_i} and the downstream coordinates p_{d_i} depend on whether the pCSR controller demands a charge or discharge for each chamber: during charge regime, $\boldsymbol{P}_u = \boldsymbol{P}_R$ and $\boldsymbol{P}_d = \boldsymbol{P}$, while in discharge regime, $\boldsymbol{P}_u = \boldsymbol{P}$ and $\boldsymbol{P}_d = \boldsymbol{P}_{\text{atm}}$, [21]. Finally, using (6), the pneumatic dynamic system (5) becomes

$$\dot{\boldsymbol{P}} + V^{-1}(\boldsymbol{q})\dot{V}(\boldsymbol{q}, \dot{\boldsymbol{q}})\boldsymbol{P} = B_p(\boldsymbol{q}, \boldsymbol{P})\boldsymbol{u} \tag{8}$$

with a positive definite pressure input matrix $B_p(\boldsymbol{q}, \boldsymbol{P}) = \rho_0 RTCV^{-1}(\boldsymbol{q})\Psi(\cdot) > 0$.

D. Dynamics in Strict Feedback Form

At this stage, tightly couplings are devised between the continuum soft robot (1) and the pneumatic system (8) stemming from the fact of the volume dependence of the generalized coordinates $\boldsymbol{q}$. It leads to establish consequently a nested dynamics in state space representation, given by

$$\ddot{\boldsymbol{q}} = f_1(\boldsymbol{q}, \dot{\boldsymbol{q}}) + g_1(\boldsymbol{q})\boldsymbol{P}, \tag{9a}$$

$$\dot{\boldsymbol{P}} = f_2(\boldsymbol{q}, \dot{\boldsymbol{q}}, \boldsymbol{P}) + g_2(\boldsymbol{q}, \boldsymbol{P})\boldsymbol{u}, \tag{9b}$$

with $f_1(\boldsymbol{q}, \dot{\boldsymbol{q}}) = -H^{-1}(\boldsymbol{q})[C(\boldsymbol{q}, \dot{\boldsymbol{q}})\dot{\boldsymbol{q}} + \boldsymbol{\tau}_{vs} + \boldsymbol{g}(\boldsymbol{q})]$, $f_2(\boldsymbol{q}, \dot{\boldsymbol{q}}, \boldsymbol{P}) = -V^{-1}(\boldsymbol{q})\dot{V}(\boldsymbol{q}, \dot{\boldsymbol{q}})\boldsymbol{P}$, $g_1(\boldsymbol{q}) = H^{-1}(\boldsymbol{q})B_q(\boldsymbol{q})$, and $g_2(\boldsymbol{q}, \boldsymbol{P}) = B_p(\boldsymbol{q}, \boldsymbol{P})$; where the term $g_1(\boldsymbol{q})\boldsymbol{P}$ is an interconnection between the dynamics. Furthermore, the system is in strict feedback form, in compliance to the backstepping control method. Hence, the control problem is stated now as follow: *"Design a pneumatic controller $\boldsymbol{u}$ using the backstepping method to guarantee global asymptotic stability of $(\boldsymbol{q}, \dot{\boldsymbol{q}})$ to $(\boldsymbol{q}^d, \dot{\boldsymbol{q}}^d) \forall (\boldsymbol{q}(0), \dot{\boldsymbol{q}}(0))$ "*.

Notice that control law $\boldsymbol{u}$ will require the inverse of B_q and of the well-posed B_p, which suggests further insight into B_q. If a set of three chambers are considered, $p = 3$, with chambers' configuration as $r_{m_i} = r_m$, and $\psi_1 = 0$, $\psi_2 = 2\pi/3$, $\psi_3 = -2\pi/3$, then input matrix adopts the following form, [16]

$$B_q(\boldsymbol{q}) = \begin{bmatrix} 1 - \kappa r_m C_\phi & 1 - \kappa r_m C_{\phi - \frac{2\pi}{3}} & 1 - \kappa r_m C_{\phi + \frac{2\pi}{3}} \\ \kappa l r_m S_\phi & \kappa l r_m S_{\phi - \frac{2\pi}{3}} & \kappa l r_m S_{\phi + \frac{2\pi}{3}} \\ -l r_m C_\phi & -l r_m C_{\phi - \frac{2\pi}{3}} & -l r_m C_{\phi + \frac{2\pi}{3}} \end{bmatrix}$$

Thus, B_q^{-1} is well-posed when three chambers for three generalized coordinates are considered, in addition, the system is fully actuated, for $\kappa > 0$.

III. Control Design

A. Open-loop Error Equation

Consider the backstepping control method for the fully actuated system (9). Let $\boldsymbol{x} = (\boldsymbol{x}_1,\ \boldsymbol{x}_2,\ \boldsymbol{x}_3)^T = (\boldsymbol{q},\ \dot{\boldsymbol{q}},\ \boldsymbol{P})^T \in \mathbb{R}^9$ be the state vector of (9), then the dynamics with state variables is written as

$$\dot{\boldsymbol{x}}_1 = \boldsymbol{x}_2, \tag{10a}$$

$$\dot{\boldsymbol{x}}_2 = -H^{-1}(\boldsymbol{x}_1)\left[h(\boldsymbol{x}_1, \boldsymbol{x}_2) + B_q(\boldsymbol{x}_1)\left(\boldsymbol{x}_3 - \boldsymbol{P}_{\text{atm}}\right)\right], \tag{10b}$$

$$\dot{\boldsymbol{x}}_3 = -V^{-1}(\boldsymbol{x}_1)\dot{V}(\boldsymbol{x}_1, \boldsymbol{x}_2)\boldsymbol{x}_3 + B_p(\boldsymbol{x}_1, \boldsymbol{x}_3)\boldsymbol{u}, \tag{10c}$$

where $h(\boldsymbol{x}_1, \boldsymbol{x}_2) = -H^{-1}(\boldsymbol{x}_1)[C(\boldsymbol{x}_1, \boldsymbol{x}_2)\boldsymbol{x}_2 + \boldsymbol{\tau}_{vs} + \boldsymbol{g}(\boldsymbol{x}_1)]$. As the control objective is the stabilization of $\boldsymbol{x}_1$ and $\boldsymbol{x}_2$, let the tracking reference vector be $\boldsymbol{x}^d = \left(\boldsymbol{x}_1^d,\ \boldsymbol{x}_2^d\right)^T \in \mathbb{R}^6$, thus the error coordinates become

$$\tilde{\boldsymbol{x}}_1 = \boldsymbol{x}_1 - \boldsymbol{x}_1^d, \tag{11a}$$

$$\tilde{\boldsymbol{x}}_2 = \boldsymbol{x}_2 - \boldsymbol{x}_2^d, \tag{11b}$$

Notice that at this point, the reference for $\boldsymbol{x}_3$ is unknown, but it depends on $\boldsymbol{x}_1$ and $\boldsymbol{x}_2$, therefore the aim is its constructive design with backstepping technique. Without loss of generality, consider the following error dynamics

$$\dot{\tilde{\boldsymbol{x}}}_1 = \tilde{\boldsymbol{x}}_2 \tag{12a}$$

$$\dot{\tilde{\boldsymbol{x}}}_2 = -H^{-1}(\boldsymbol{x}_1)\left[h(\boldsymbol{x}_1, \boldsymbol{x}_2) + B_q(\boldsymbol{x}_1)\left(\boldsymbol{x}_3 - \boldsymbol{P}_{\text{atm}}\right)\right] - \dot{\boldsymbol{x}}_2^d \tag{12b}$$

$$\dot{\boldsymbol{x}}_3 = -V^{-1}(\boldsymbol{x}_1)\dot{V}(\boldsymbol{x}_1, \boldsymbol{x}_2)\boldsymbol{x}_3 + B_p(\boldsymbol{x}_1, \boldsymbol{x}_3)\boldsymbol{u}. \tag{12c}$$

Next, the backstepping is developed twice for the velocity error $\tilde{\boldsymbol{x}}_2$ and the pressure $\boldsymbol{x}_3$ as virtual controllers to finally compute a control u for (12), and then we prove the asymptotic stability $(\tilde{\boldsymbol{x}}_1, \tilde{\boldsymbol{x}}_2) \to 0$ as $t \to \infty$, in the sense of Lyapunov.

B. Backstepping Control Design

Without loss of generality, assume a disturbance free system, full knowledge of model and its parameters, and full access to the state variables. In these circumstances:

1) Step 1: Let the change of coordinates be $\boldsymbol{z}_1 = \tilde{\boldsymbol{x}}_1$, where $\boldsymbol{z}_1$ is an error variable, then subsystem (12a) can be rewritten as follows

$$\dot{\boldsymbol{z}}_1 = \tilde{\boldsymbol{x}}_2. \tag{13}$$

If $\tilde{\boldsymbol{x}}_2 = \omega_1$ acts as a stabilizing function for (13), then consider

$$\omega_1 \triangleq -K_1 \boldsymbol{z}_1, \tag{14}$$

with $K_1 = K_1^T > 0$. It is easy to show that z_1 is stabilized at the origin. Therefore, an error variable $\boldsymbol{z}_2$ is defined as follows

$$\boldsymbol{z}_2 = \tilde{\boldsymbol{x}}_2 - \omega_1, \tag{15}$$

whose origin implies $\tilde{\boldsymbol{x}}_2 = \omega_1$. Equation (15) suggests to write the state variable $\tilde{\boldsymbol{x}}_2 = \boldsymbol{z}_2 + \omega_1$, which substituting it into (13), one obtains

$$\dot{\boldsymbol{z}}_1 = \boldsymbol{z}_2 - K_1 \boldsymbol{z}_1. \tag{16}$$

Stability of $\boldsymbol{z}_1$-dynamics is verified considering the following Lyapunov candidate function

$$V_1 = \frac{1}{2} \boldsymbol{z}_1^T \boldsymbol{z}_1,$$

whose time derivative along solutions (16) yields

$$\dot{V}_1 = -\boldsymbol{z}_1^\intercal K_1 \boldsymbol{z}_1 + \boldsymbol{z}_1^\intercal \boldsymbol{z}_2. \tag{17}$$

If $\boldsymbol{z}_2 \to 0$, (17) shows the global asymptotic stability for $\boldsymbol{z}_1$. This is precisely the objective of the next step.

2) Step 2: Dynamics of error variable $\boldsymbol{z}_2$ is obtained by the time derivative of (15), that is $\dot{\boldsymbol{z}}_2 = \dot{\tilde{\boldsymbol{x}}}_2 - \dot{\omega}_1$, then, using (12b), it becomes

$$\begin{aligned} \dot{\boldsymbol{z}}_2 = &- H^{-1}(\boldsymbol{x}_1) \left[h(\boldsymbol{x}_1, \boldsymbol{x}_2) + B_q(\boldsymbol{x}_1) \left[\boldsymbol{x}_3 - \boldsymbol{P}_{\text{atm}} \right] \right] \\ &- \dot{\boldsymbol{x}}_2^d - \dot{\omega}_1. \end{aligned} \tag{18}$$

Now, let $\boldsymbol{x}_3 = \omega_2$ act as a stabilizing function for the dynamics (18) aimed at stabilizing $\boldsymbol{z}_2$. To this end, let $\boldsymbol{z}_3$ define the error coordinate as follows

$$\boldsymbol{z}_3 = \boldsymbol{x}_3 - \omega_2, \tag{19}$$

whose origin implies $\boldsymbol{x}_3 = \omega_2$. Using (19), dynamics (18) becomes

$$\begin{aligned} \dot{\boldsymbol{z}}_2 = &- H^{-1}(\boldsymbol{x}_1) \left[h(\boldsymbol{x}_1, \boldsymbol{x}_2) \right] - \dot{\boldsymbol{x}}_2^d - \dot{\omega}_1 \\ &- H^{-1}(\boldsymbol{x}_1) B_q(\boldsymbol{x}_1) \boldsymbol{P}_{\text{atm}} + H^{-1}(\boldsymbol{x}_1) B_q(\boldsymbol{x}_1) \left[\boldsymbol{z}_3 + \omega_2 \right] \end{aligned} \tag{20}$$

In this way, stabilizing function ω_2 is designed to guarantee stability for $\boldsymbol{z}_2$ dynamics using the following Lyapunov candidate function

$$V_2 = V_1 + \frac{1}{2} \boldsymbol{z}_2^\intercal \boldsymbol{z}_2,$$

whose time derivative along the solutions of (20) yields

$$\begin{aligned} \dot{V}_2 = &-\boldsymbol{z}_1^\intercal K_1 \boldsymbol{z}_1 + \boldsymbol{z}_2^\intercal \big[\boldsymbol{z}_1 - H^{-1}(\boldsymbol{x}_1) \left[h(\boldsymbol{x}_1, \boldsymbol{x}_2) \right] - \dot{\boldsymbol{x}}_2^d - \dot{\omega}_1 \\ &- H^{-1}(\boldsymbol{x}_1) B_q(\boldsymbol{x}_1) \boldsymbol{P}_{\text{atm}} + H^{-1}(\boldsymbol{x}_1) B_q(\boldsymbol{x}_1) \left[\boldsymbol{z}_3 + \omega_2 \right] \big] \end{aligned} \tag{21}$$

Now, consider the following stabilizing function ω_2

$$\begin{aligned} \omega_2 = &B_q^{-1}(\boldsymbol{x}_1) H(\boldsymbol{x}_1) \big[\dot{\omega}_1 + \dot{\boldsymbol{x}}_2^d + H^{-1}(\boldsymbol{x}_1) [h(\boldsymbol{x}_1, \boldsymbol{x}_2)] \\ &- \boldsymbol{z}_1 - K_2 \boldsymbol{z}_2 \big] + \boldsymbol{P}_{\text{atm}}, \end{aligned} \tag{22}$$

with $K_2 = K_2^T > 0$. Substituting (22) into (21), we obtain

$$\dot{V}_2 = -\boldsymbol{z}_1^\intercal K_1 \boldsymbol{z}_1 - \boldsymbol{z}_2^\intercal K_2 \boldsymbol{z}_2 + \boldsymbol{z}_2^\intercal H^{-1}(\boldsymbol{x}_1) B_q(\boldsymbol{x}_1) \boldsymbol{z}_3, \tag{23}$$

Notice that if $\boldsymbol{z}_3 \to 0$, then $(\boldsymbol{z}_1, \boldsymbol{z}_2) \to (0, 0)$. That is the objective of next step.

3) Step 3: Using (10c), the time derivative of (19) can be written as follows

$$\begin{aligned} \dot{\boldsymbol{z}}_3 &= \dot{\boldsymbol{x}}_3 - \dot{\omega}_2 \\ &= -V^{-1}(\boldsymbol{x}_1) \dot{V}(\boldsymbol{x}_1, \boldsymbol{x}_2) \boldsymbol{x}_3 + B_p(\boldsymbol{x}_1, \boldsymbol{x}_3) \boldsymbol{u} - \dot{\omega}_2 \end{aligned} \tag{24}$$

Consider the following Lyapunov candidate function

$$V_3 = V_2 + \frac{1}{2} \boldsymbol{z}_3^\intercal \boldsymbol{z}_3, \tag{25}$$

whose time derivative along (24) is

$$\begin{aligned} \dot{V}_3 = &-\boldsymbol{z}_1^\intercal K_1 \boldsymbol{z}_1 - \boldsymbol{z}_2^\intercal K_2 \boldsymbol{z}_2 + \boldsymbol{z}_3^\intercal \big[B(\boldsymbol{x}_1) H^{-\intercal}(\boldsymbol{x}_1) \boldsymbol{z}_2 \\ &- V^{-1}(\boldsymbol{x}_1) \dot{V}(\boldsymbol{x}_1, \boldsymbol{x}_2) \boldsymbol{x}_3 + B_p(\boldsymbol{x}_1, \boldsymbol{x}_3) \boldsymbol{u} - \dot{\omega}_2 \big]. \end{aligned} \tag{26}$$

Finally, let the control law $\boldsymbol{u}$ be

$$\begin{aligned} \boldsymbol{u} = B_p^{-1}(\boldsymbol{x}_1, \boldsymbol{x}_3) \big[&\dot{\omega}_2 + V^{-1}(\boldsymbol{x}_1) \dot{V}(\boldsymbol{x}_1, \boldsymbol{x}_2) \boldsymbol{x}_3 \\ &- B_q(\boldsymbol{x}_1) H^{-\intercal}(\boldsymbol{x}_1) \boldsymbol{z}_2 - K_3 \boldsymbol{z}_3 \big], \end{aligned} \tag{27}$$

with $K_3 = K_3^T > 0$. Substituting (27) into (26), one obtains

$$\dot{V}_3 = -\boldsymbol{z}_1^\intercal K_1 \boldsymbol{z}_1 - \boldsymbol{z}_2^\intercal K_2 \boldsymbol{z}_2 - \boldsymbol{z}_3^\intercal K_3 \boldsymbol{z}_3, \tag{28}$$

which is negative definite, then implying the global asymptotic stability of origin $(\boldsymbol{z}_1, \boldsymbol{z}_2, \boldsymbol{z}_3) = (0, 0, 0)$. Notice that (25) can be rewritten as $V_3 = \frac{1}{2} \boldsymbol{z}^T \boldsymbol{z}$, for $\boldsymbol{z} = (\boldsymbol{z}_1,\ \boldsymbol{z}_2,\ \boldsymbol{z}_3)^T \in \mathbb{R}^9$, and a diagonal block matrix $K \in \mathbb{R}^{9 \times 9}$ whose entries are K_1, K_2, K_3; then (28) can be rewritten as

$$\begin{aligned} \dot{V}_3 &= -\boldsymbol{z}^\intercal K \boldsymbol{z} \\ &\leq -\lambda_m(K) \|z\|^2 \\ &\leq -2\lambda_m(K) V_3 \end{aligned} \tag{29}$$

where $\lambda_m(*)$ represents the minimum eigenvalue $(*)$ Solving (29), one obtains

$$V_3(t) \leq V_0 \mathrm{e}^{-2\lambda_m(K)(t - t_0)}, \tag{30}$$

where $V_0 = V(0)$, showing the exponential convergence of error variables $\boldsymbol{z}$.

Consequently, it can be concluded that

$$\begin{pmatrix} \tilde{\boldsymbol{x}}_1 \\ \tilde{\boldsymbol{x}}_2 \\ \boldsymbol{x}_3 \end{pmatrix} \xrightarrow[t \to \infty]{} \begin{pmatrix} 0 \\ \omega_1 \\ \omega_2 \end{pmatrix}.$$

According to (14), given that ω_1 depends on $\boldsymbol{z}_1$, then

$$\begin{pmatrix} \tilde{\boldsymbol{x}}_1 \\ \tilde{\boldsymbol{x}}_2 \\ \boldsymbol{x}_3 \end{pmatrix} \xrightarrow[t\to\infty]{} \begin{pmatrix} 0 \\ 0 \\ \omega_2 \end{pmatrix}.$$

If $(\tilde{\boldsymbol{x}}_1, \tilde{\boldsymbol{x}}_2)^T \to 0$, then $(\boldsymbol{x}_1, \boldsymbol{x}_2)^T \to (\boldsymbol{x}_1^d, \boldsymbol{x}_2^d)^T$. Evaluating ω_2 (22) in $(\boldsymbol{x}_1^d, \boldsymbol{x}_2^d)^T$ the desired absolute pressure is obtained

$$\begin{aligned} \omega_2^* &= B^{-1}(\boldsymbol{x}_1^d)\tau^d + \boldsymbol{P}_{\text{atm}} \\ \omega_2^* &= \boldsymbol{P}_r^d + \boldsymbol{P}_{\text{atm}}. \end{aligned} \tag{31}$$

Therefore, we have proved the main result.

Theorem 1. *Closed-loop dynamics* (12) *with control* (27)*, and stabilizing functions* (14)*,* (22)*, guarantee exponential convergence of the error variables* $\boldsymbol{z}$ *and so does* $(\Delta\boldsymbol{x}_1, \Delta\boldsymbol{x}_2) \to (0, 0)$*, as well as the pressure to the stabilizing function* $\boldsymbol{x}_3 \to \omega_2$*, ensuring globally asymptotically* $(\boldsymbol{x}_1, \boldsymbol{x}_2) \to (\boldsymbol{x}_1^d, \boldsymbol{x}_2^d)$.

IV. Simulations

A. The Simulator

Simulations were conducted in Matlab Simulink R2021b, on a PC equipped with Intel Core i5-1135G7 and 12 GB of RAM, running with a 0.0001-maximum step size variable-step integrator ODE23tb solver.

1) Reference Trajectories: The reference trajectory is defined as $\boldsymbol{q}^d = [l^d, -1.0472, \kappa^d]^T$ where the desired azimuth angle is constant and both l^d and κ^d vary exponentially, this reference trajectory represents changes in length and curvature in the same plane at the constant azimuth. The first ten seconds l^d and κ^d increase exponentially, which implies pressurization in the pneumatic chambers (charge regime), and the final ten seconds l^d and κ^d decrease exponentially (discharge regime).

2) Parameters and Initial Conditions: Parameters of the pneumatic soft robot and the pneumatic system are $r_{ch} = 0.002$(m), $r_m = 0.0075$(m), $r_e = 0.015$(m), $m = 0.0544$(Kg), $T = 293$(K), $R = 287.05$(J/Kg·K), $b = 0.528$, $C = 3.7 \times 10^{-10}$(m^3/Pa·s), $P_{\text{atm}} = 101500$(Pa), $P_R = 204921$(Pa), and $\rho_0 = 1.2068$(Kg/m^3). The parameters r_{ch}, r_m, r_e, and m are from a physical soft robot used in the work of [16]. Parameters R, P_{atm} and ρ_0, are standard thermodynamic values for the air at sea-level atmospheric pressure and the reservoir pressure P_R was proposed sufficiently large. The values of C and b were selected from a solenoid valve used for soft actuators in the work of [21]. The initial conditions of the generalized coordinates $\boldsymbol{q}$ are $l_0 = 0.072$ (m), $\phi_0 = 0$ (rad), and $\kappa_0 = 0.069$ (1/m). Feedback control gains $K_1 = K_2 = K_3 = \text{diag}(180, 180, 180)$ were obtained in congruence with the stability tests detailed in Section III, approaching the value used by trial and error.

B. Results

The tracking of the configuration coordinates of the pCSR is shown in Fig. 2, which at $t = 0$, the start of the charge regime, shows that the backstepping controller performs the tracking with no overshooting. However, at $t = 10$, under the discharge regime, there is a visible transient response in the

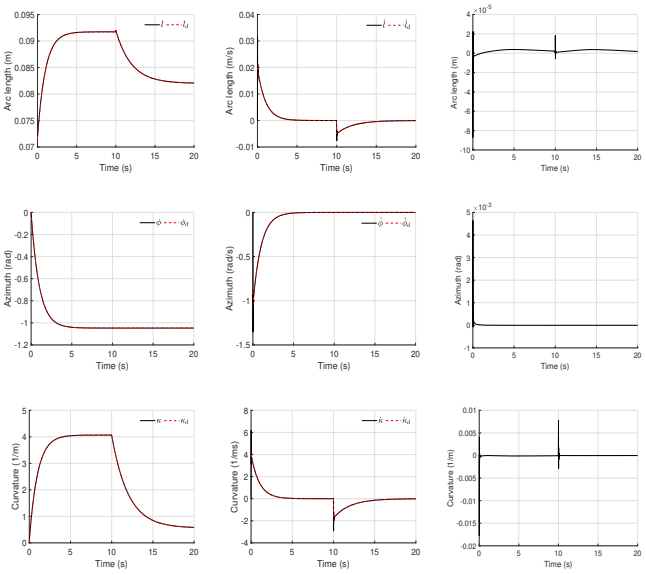

Fig. 2. Soft robot system: Configuration (deformation) coordinates are shown in the left column, with its generalized velocities in the middle column, and tracking errors in the right column. Rows show from top to bottom length, azimuth, and curvature, respectively, and it can be seen that at $t = 10$ s the system switches from charge to a discharge regime.

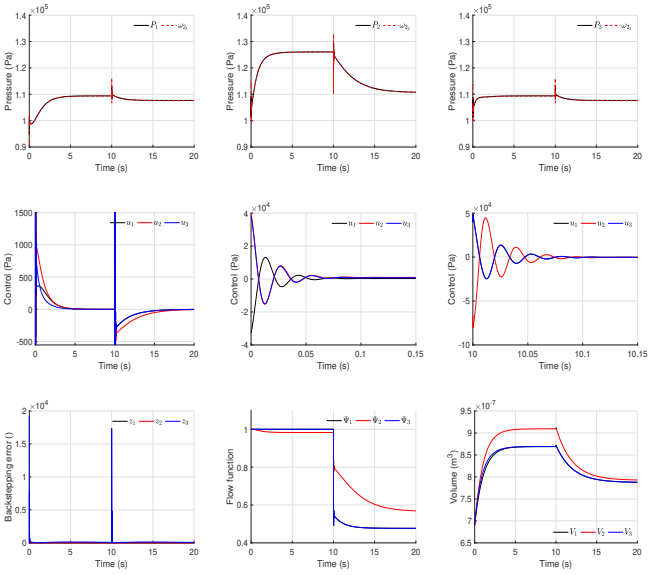

Fig. 3. Pneumatic actuation system and control: Chambers' pressures (first row), pressure control $\boldsymbol{u}$ and zooms to the transients at the start of charge $t = 0$ s and discharge $t = 10$ s regimes (second row), error variables $\boldsymbol{z}$ from the backstepping design, flow function Ψ and pressure chambers' volume (third row).

columns of configuration derivatives and configuration error. In practice, the transient would also appear as a consequence of the *ON/OFF* change in a typical industrial solenoid valve.

Fig. 3 shows the control signals and induced input pressures. The desired constant azimuth implies a pressure increase in all three chambers simultaneously, but a higher one in only one of them, see first row and second column, corresponding to the second chamber. In the same row, the stabilizing function

ω_2 acts as the reference pressures for the chambers, where the backstepping controller performs tracking despite the transient induced by flow regime change at $t = 10s$. Second row shows the control signal behavior $\boldsymbol{u}$. In the first column steady state shows how control varies to produce pressure tracking (with the backstepping errors just in the row below). Second and third columns show transients of both charge and discharge regimes which exhibit exponential convergence with similar overshoot and settling times, about $100ms$. The switching of flow regime can be seen in last row second column, where during charge regime the flow is nearly or even chocked for all three chambers while during the discharge regime the three pneumatic chambers present an evident subsonic flow. Finally, volumes are shown in last row, third column, exhibiting a continuous behavior, even at flow regime change.

V. Discussions

The flow function (7) imposes a hard nonlinearity in the penumatic systems, which induce a control switching conditions since downstream $\boldsymbol{P}_d$ and upstream $\boldsymbol{P}_u$ pressures commute, even if this function is continuous. Therefore, commuting implies a switching dynamical behavior for each regime, this issue deserves further consideration. See for instance an analytical definition [18], or a simplified expression [20], the dependence of the function changes whether the pneumatic actuator is in charge or discharge regime. These regimes have not been addressed in the literature of pneumatic control for soft robots, an issue beyond the scope of this manuscript but a necessary one to study when realizing experiments of pCSR actuated by solenoid valves. Such commutation is observed in simulations as induced transients in control and state. The transients are faster than the ones obtained in our previous work [8]; however, they still present a relative slow settling time, which indicates that such phenomena must not be neglected in practice.

Our scheme yields the global stability with a sound constructive scheme, however one drawback is that it is model dependent, which can be ameliorated with an adaptive backstepping scheme, at the expense of requiring a regressor, or a neural network backstepping.

VI. Conclusions

The configuration tracking of a pneumatic continuum soft robot is addressed with a model-based backstepping control, considering the full dynamics of both subsystems. The proposed backstepping control guarantees tracking, with stability in the sense of Lyapunov, based on a constructive method to design the reference pressure for the pneumatic dynamics.

Simulations show the expected exponential convergence of errors considering realistic parameters corresponding to an experimental scenario of a real prototype system. A transient response appears at the beginning of both charge and discharge regimes, but the settling time and overshoot magnitudes remain under the acceptable margins for practical implementation.

Future work includes the design of a robust backstepping design approach as well as a model-free version, with an efficient neural network backstepping. In addition, experimental testbed, including pneumatic instrumentation and soft robot manufacture, is under way to asses its real time performance.

References

[1] V. Falkenhahn, A. Hildebrandt, R. Neumann, and O. Sawodny, "Dynamic control of the bionic handling assistant," *IEEE/ASME Transactions on Mechatronics*, vol. 22, no. 1, pp. 6–17, 2016.

[2] T. George Thuruthel, Y. Ansari, E. Falotico, and C. Laschi, "Control strategies for soft robotic manipulators: A survey," *Soft robotics*, vol. 5, no. 2, pp. 149–163, 2018.

[3] E. H. Skorina, M. Luo, W. Tao, F. Chen, J. Fu, and C. D. Onal, "Adapting to flexibility: model reference adaptive control of soft bending actuators," *IEEE Robotics and Automation Letters*, vol. 2, no. 2, pp. 964–970, 2017.

[4] C. Della-Santina, A. Bicchi, and D. Rus, "Dynamic control of soft robots with internal constraints in the presence of obstacles," *IEEE/RJS Internation Conference on Intelligent Robots and Systems*, 2019.

[5] M. Smaoui, X. Brun, and D. Thomasset, "A study on tracking position control of an electropneumatic system using backstepping design," *Control Engineering Practice*, vol. 14, no. 8, pp. 923–933, 2006.

[6] A. D. Marchese and D. Rus, "Design, kinematics, and control of a soft spatial fluidic elastomer manipulator," *The International Journal of Robotics Research*, vol. 35, no. 7, pp. 840–869, 2016.

[7] C. Della Santina, C. Duriez, and D. Rus, "Model based control of soft robots: A survey of the state of the art and open challenges," *arXiv preprint arXiv:2110.01358*, 2021.

[8] J. E. Ayala-Carrillo, V. Parra-Vega, E. Olguín-Díaz, and C. A. Trejo-Ramos, "Cascade control for robust tracking of continuum soft robots with finite-time convergence of pneumatic system," *IEEE Control Systems Letters*, 2022.

[9] P. V. Kokotovic, "The joy of feedback: nonlinear and adaptive," *IEEE Control Systems Magazine*, vol. 12, no. 3, pp. 7–17, 1992.

[10] R. Sepulchre, M. Jankovic, and P. V. Kokotovic, *Constructive nonlinear control*. Springer Science & Business Media, 2012.

[11] H. Ramirez-Rodriguez, V. Parra-Vega, A. Sanchez-Orta, and O. Garcia-Salazar, "Robust backstepping control based on integral sliding modes for tracking of quadrotors," *Journal of Intelligent & Robotic Systems*, vol. 73, no. 1, pp. 51–66, 2014.

[12] T. Wang, Y. Zhang, and Z. Chen, "Design and verification of model-based nonlinear controller for fluidic soft actuators," in *2018 IEEE/ASME International Conference on Advanced Intelligent Mechatronics (AIM)*. IEEE, 2018, pp. 1178–1183.

[13] E. Franco, T. Ayatullah, A. Sugiharto, A. Garriga-Casanovas, and V. Virdyawan, "Nonlinear energy-based control of soft continuum pneumatic manipulators," *Nonlinear Dynamics*, vol. 106, no. 1, pp. 229–253, 2021.

[14] M. Stölzle and C. Della Santina, "Piston-driven pneumatically-actuated soft robots: modeling and backstepping control," *IEEE Control Systems Letters*, vol. 6, pp. 1837–1842, 2021.

[15] H. Huang, J. Lin, L. Wu, B. Fang, and F. Sun, "Optimal control scheme for pneumatic soft actuator under comparison of proportional and pwm-solenoid valves," *Photonic Network Communications*, vol. 37, no. 2, pp. 153–163, 2019.

[16] C. Trejo-Ramos, E. Olguín-Díaz, V. Parra-Vega, and C. Vázquez-García, "A lagrangian dynamic model for soft cylindrical robots without internal holonomic constraint." *Latin American Robotics Symposium (LARS)*, pp. 132–137, 2021.

[17] M.-J. Potvin, J.-C. Piedboeuf, and J. A. Nemes, "Comparison of viscoelastic models in simulating the transient response of a slewing polymer arm," *Journal of Dynamic Systems, Measurement, and Control*, vol. 120, no. 3, pp. 340–345, 09 1998.

[18] E. Richer and Y. Hurmuzlu, "A high performance pneumatic force actuator system: Part i—nonlinear mathematical model," *J. dyn. sys., meas., control*, vol. 122, no. 3, pp. 416–425, 2000.

[19] T. R. Young, M. S. Xavier, Y. K. Yong, and A. J. Fleming, "A control and drive system for pneumatic soft robots: Pneusord," in *2021 IEEE/RSJ International Conference on Intelligent Robots and Systems (IROS)*. IEEE, 2020, pp. 2822–2829.

[20] P. Beater, *Pneumatic drives*. Springer, 2007.

[21] M. S. Xavier, A. J. Fleming, and Y. K. Yong, "Design and control of pneumatic systems for soft robotics: a simulation approach," *IEEE Robotics and Automation Letters*, vol. 6, no. 3, pp. 5800–5807, 2021.